Influence of the Oscillator Equivalent Circuit on the Stable Modes of Parallel-Coupled Oscillators

Heng-Chia Chang, Eric S. Shapiro, *Member, IEEE*, and Robert A. York, *Member, IEEE*

***Abstract*— This paper addresses a deficiency in the authors' previous work on coupled-oscillator theory, involving the nature of the resonance in the oscillator equivalent circuit and its influence on the stable modes of the coupled-oscillator system. The authors show that series and parallel oscillators with identical free-running characteristics nevertheless behave differently when coupled by the same coupling network. The analysis focuses on parallel-coupling networks, which are most practical at microwave frequencies, and specifically on nearest-neighbor coupling topologies. The theory is verified using four small active-patch arrays operating at 10 GHz.**

***Index Terms*—Broadside pattern, coupling phase, endfire pattern, oscillator model, parallel coupled, parallel oscillator, series oscillator.**

I. Introduction

SPATIAL combining techniques can be used to combine microwave and millimeter-wave sources, provided the array elements are mutually coherent. Mutual injection-locking techniques are one possible method for achieving synchronous operation of the array elements. An attractive feature of injection-locking techniques is the ability to manipulate the phase distribution without additional phase-shifting circuitry.

The dynamics of such arrays and application to beam scanning has been described in prior literature [1]–[8]. In [4], a series-resonator model for the oscillator was employed in the analysis, whereas [5], [8] used a parallel-resonator-equivalent circuit. In both cases, the duality between series and parallel networks was noted, and used to argue for a similarity in the dynamics of arrays of oscillators of either type. However, implicit in this argument was the requirement that each type of oscillator requires the corresponding coupling topology, i.e., oscillators with series-equivalent circuits should be coupled in series, whereas parallel oscillators should be coupled in parallel. At microwave frequencies, both series and parallel oscillators are common, but practical coupling schemes usually involve connecting oscillators in parallel, since the oscillators typically share a common ground.

In this paper, the dynamics of parallel-coupled oscillators are examined. The individual oscillators are modeled using either a series- or parallel-resonator circuit. Significant differences are found in the dynamics for a given coupling scheme, leading to different stable-phase distributions for each case. The analysis focuses specifically on a simple nearest-neighbor coupling topology used in previous analytical and experimental work [5]. The theory is verified using four separate three-element MESFET oscillator arrays at X-band, which represent the four permutations of either series or parallel equivalents and two different coupling configurations.

Manuscript received December 13, 1996; revised April 25, 1997. This work was supported by Hughes Research Laboratories, Malibu, CA, and the U.S. Army Research Office.

The authors are with the Department of Electrical and Computer Engineering, University of California at Santa Barbara, CA 93106 USA.

Publisher Item Identifier S 0018-9480(97)05379-9.

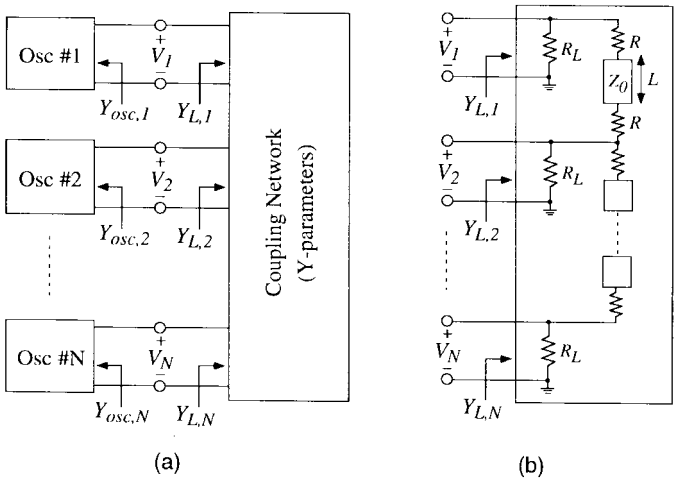

Fig. 1. (a) N-oscillator system coupled through an arbitrary N-port network described by Y-parameters. (b) A common nearest-neighbor coupling network, which connects the oscillators in parallel, and allows the coupling strength and coupling phase to be easily manipulated.

II. Dynamics of Parallel-Coupled Oscillators

Previous analysis of coupled-oscillator systems [5] like that in Fig. 1(a) have shown that the amplitude and phase dynamics of an N-oscillator system can be adequately modeled by the following set of coupled first-order differential equations:

$$\frac{\partial A_i}{\partial t} = A_i \mathrm{Re}\{F_i(\bar{A},\bar{\theta})\} \tag{1}$$

$$\frac{\partial \theta_i}{\partial t} = \omega_i + \mathrm{Im}\{F_i(\bar{A},\bar{\theta})\}, \qquad i = 1,2,\cdots,N \tag{2}$$

where A_i, θ_i, and ω_i are the amplitude, instantaneous phase, and free-running frequency of the ith oscillator, respectively, and

$$F_i(\bar{A},\bar{\theta}) \simeq -\left(\frac{\partial Y_{\mathrm{osc},i}(\omega_i,A_i)}{\partial(j\omega)}\right)^{-1}[Y_{\mathrm{osc},i}(\omega_i,A_i)+Y_{L,i}(\omega_i)]. \tag{3}$$

In this formulation, it is assumed that the frequency dependence of the coupling admittance matrix is negligible

compared to the oscillator circuits; i.e., the oscillator circuits have a higher Q-factor than the coupling network.

A stable steady-state solution to (1) and (2), denoted as $(\bar{\bar{A}}, \bar{\bar{\theta}})$, requires that $\partial A_i/\partial t = 0$ and $\partial\theta_i/\partial t = \omega$ for all i, where ω is the (unknown) steady-state oscillation frequency for the system. The steady-state is, therefore, found by solving

$$F_i(\bar{\bar{A}}, \bar{\bar{\theta}}) = \jmath(\omega - \omega_i), \qquad i = 1, 2, \cdots, N \tag{4}$$

which represents a set of $2N$ equations with $2N$ unknowns (one of the phases is arbitrary). The stability of these solutions can be investigated by perturbing the dynamic equations (1), (2) around the solutions of (4), as described in [5], [8]. The analysis is now one of specifying the function F. At the ith port, the oscillator load is given by

$$Y_{L,i} = \sum_{j=1}^{N} Y_{ij} \frac{A_j}{A_i} e^{\jmath(\theta_j - \theta_i)} \tag{5}$$

where Y_{ij} is the admittance matrix of the coupling network. A simple coupling network that is appropriate for planar oscillator circuits is shown in Fig. 1(b). When the coupling resistance is chosen such that $R = Z_0$, this network has the following admittance parameters [5]:

$$Y_{ij} = \begin{cases} \dfrac{\eta_i}{2Z_0} + G_L, & i = j \\ \dfrac{-e^{-\jmath\beta L}}{2Z_0}, & |i-j| = 1 \\ 0, & \text{otherwise} \end{cases}$$

$$\frac{\partial Y_{ij}}{\partial(\jmath\omega)} = \begin{cases} 0, & i = j \\ \dfrac{\tau_g e^{-\jmath\beta L}}{2Z_0}, & |i-j| = 1 \\ 0, & \text{otherwise} \end{cases} \tag{6}$$

where βL is the electrical length of the transmission line, Z_0 is the characteristic impedance, $\eta_i = (2 - \delta_{i1} - \delta_{iN})$, δ_{ij} is the Kronecker delta function, and τ_g is the group delay through the transmission line. For TEM or quasi-TEM lines, $\tau_g = \beta L/\omega$, and when $\beta L \leq 2\pi$, then the assumptions leading to (3) are satisfied if $\pi R_L/QZ_0 \ll 1$ $(R_L = 1/G_L)$ [5]. It will be assumed that this constraint holds, and the following *coupling parameters* for future convenience defined as

$$\varepsilon \equiv \frac{R_L}{2Z_0} \quad \text{and} \quad \Phi \equiv \beta L. \tag{7}$$

To proceed further, an oscillator model needs to be specified. In a well-designed oscillator, the oscillation frequency will occur in the vicinity of a reactance or susceptance null, which is assumed to be well isolated from other nulls (spectrally) to avoid mode-hopping or multifrequency operation. In a narrow range of frequencies around such a resonance, the oscillator circuit can be modeled by either a parallel- or series-resonant circuit, shown in Fig. 2(a) and (b), respectively. For stability in the free-running case, the device in the parallel model must have a negative *conductance*, which decreases with increasing oscillation amplitude. The device in the series model must have a negative *resistance*, which decreases in magnitude with increasing oscillation amplitude. It is assumed that the array is composed of such oscillators which are stable in their free-running state. The coupling between the oscillators serves only to synchronize the frequencies via the injection-locking phenomenon, and results in only a slight perturbation of the oscillators from the free-running configuration.

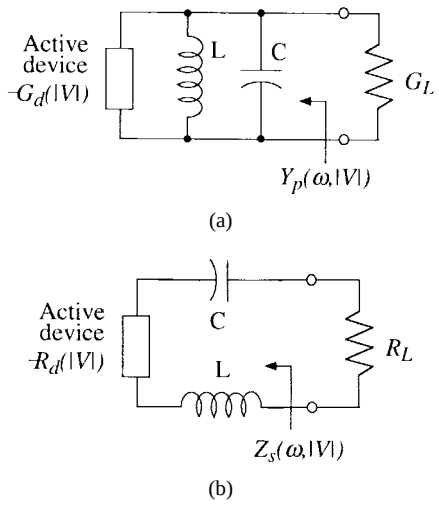

Fig. 2. Equivalent circuits of oscillator models. (a) Parallel-resonant circuit. (b) Series-resonant circuit.

A. Dynamics with Parallel-Oscillator Model

Using the parallel model of Fig. 2(a), the input admittance of the ith oscillator near the resonant frequency ω_i can be approximated as

$$Y_{\text{osc},i} \approx -G_d(A_i) + \jmath 2C_i(\omega - \omega_i) \tag{8}$$

where C_i is the shunt capacitance. In the free-running state, the oscillator feeds a load conductance of G_L as shown, so a Q-factor can be defined for the free-running oscillator as $Q = \omega_i R_L C_i$, and write

$$Y_{\text{osc},i} \approx -G_d(A_i) + \jmath\frac{G_L}{\omega_{3\,\text{dB}}}(\omega - \omega_i) \tag{9}$$

where $\omega_{3\,\text{dB}} = \omega_i/2Q$ is half the 3-dB bandwidth of the oscillator tank circuit. It is assumed that the oscillators can have slightly different free-running frequencies, but that the Q-factors and 3-dB bandwidths are all the same—to first order. From this, one sees that

$$\frac{\partial Y_{\text{osc},i}(\omega_i)}{\partial(\jmath\omega)} = \frac{G_L}{\omega_{3\,\text{dB}}}. \tag{10}$$

Here, a simple Van der Pol nonlinearity is assumed, which leads to sinusoidal oscillations

$$-G_d(A) = -G_0 + G_2 A^2 \tag{11}$$

where $-G_0$ is the small-signal negative conductance, and G_2 describes the saturation of the negative conductance. In the free-running state where the oscillator feeds a load conductance of G_L, the oscillation conditions allow one to write [5]

$$1 - G_d(A_i)/G_L = -\mu_p\left(1 - A_i^2/\alpha_i^2\right) \tag{12}$$

where α_i is the free-running oscillation amplitude, and μ_p is a dimensionless nonlinearity parameter for the parallel oscillator related to G_2 and G_L.

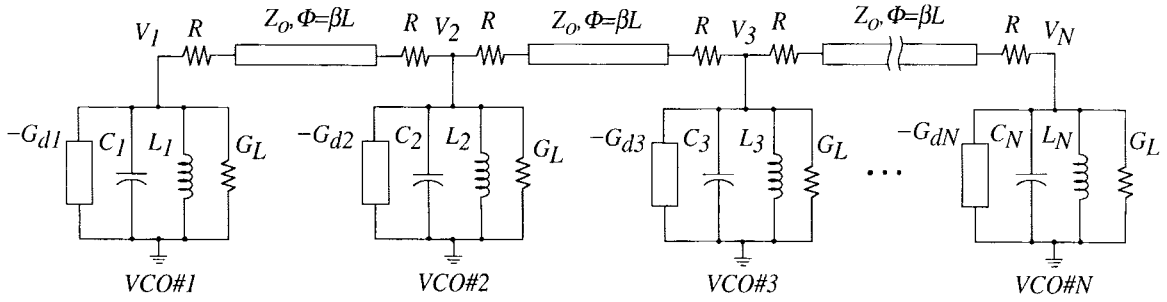

Fig. 3. Schematic diagram of N-parallel-coupled oscillators modeled by parallel-resonant circuits.

Using (5), (9), and (10), the function F_i from (3) is then given by

$$F_i = -\frac{\omega_{3\,\mathrm{dB}}}{G_L}\left[-G_d(A_i) + \sum_{j=1}^{N} Y_{ij}\frac{A_j}{A_i}e^{\jmath(\theta_j-\theta_i)}\right]. \tag{13}$$

Substituting (6) and (12) into (13), the array amplitude and phase dynamics from (1) and (2) become

$$\frac{\partial A_i}{\partial t} = \omega_{3\,\mathrm{dB}}A_i\left[\mu_p\left(1-A_i^2/\alpha_i^2\right)-\eta_i\epsilon\right] + \epsilon\omega_{3\,\mathrm{dB}}\sum_{\substack{j=i-1\\ j\neq i}}^{i+1} A_j\cos(\theta_i-\theta_j+\Phi) \tag{14}$$

$$\frac{\partial\theta_i}{\partial t} = \omega_i - \epsilon\omega_{3\,\mathrm{dB}}\sum_{\substack{j=i-1\\ j\neq i}}^{i+1}\frac{A_j}{A_i}\sin(\theta_i-\theta_j+\Phi), \quad i=1,2,\cdots,N. \tag{15}$$

When applied to the end elements in the array ($i=1$ or $i=N$), $A_0 = A_{N+1} = 0$ must be defined. These equations are the same as those derived in [4], and correspond to the array depicted in Fig. 3.

B. Dynamics with Series-Oscillator Model

The dynamics for a series-oscillator model can be derived in similar fashion. Close to the resonant frequency, the input impedance of the oscillator in Fig. 2(b) is given by

$$Z_{\mathrm{osc},\,i} \approx -R_d(A_i) + \jmath\frac{R_L}{\omega_{3\,\mathrm{dB}}}(\omega-\omega_i). \tag{16}$$

A simple Van der Pol nonlinearity is again presumed

$$-R_d(A_i) \approx -R_0 + R_2A^2 \tag{17}$$

so that

$$1 - R_d(A_i)/R_L = -\mu_s\left(1-A_i^2/\alpha_i^2\right) \tag{18}$$

where μ_s is a dimensionless nonlinearity parameter for the series oscillator, related to R_2 and R_L.

This paper's formulation requires the input *admittance* and derivative with frequency evaluated at the free-running frequency, which are found to be

$$Y_{\mathrm{osc},\,i}(\omega_i) \approx \frac{-1}{R_d(A_i)}$$
$$\frac{\partial Y_{\mathrm{osc},\,i}(\omega_i)}{\partial(\jmath\omega)} = -\frac{R_L}{\omega_{3\,\mathrm{dB}}R_d^2(A_i)}. \tag{19}$$

Combining (3) , (5), and (19) gives

$$F_i = \omega_{3\,\mathrm{dB}}\frac{R_d^2(A_i)}{R_L}\left[\frac{-1}{R_d(A_i)} + \sum_{j=1}^{N} Y_{ij}\frac{A_j}{A_i}e^{\jmath(\theta_j-\theta_i)}\right] \tag{20}$$

which is then substituted into (1) and (2). In this case, note that when the oscillators are only slightly perturbed from their free-running state, the amplitudes should stay relatively close to the free-running amplitudes, and, therefore, $R_d/R_L \approx -1+\delta$, where δ represents a small number. Keeping only leading terms in this approximation gives

$$\frac{\partial A_i}{\partial t} = \omega_{3\,\mathrm{dB}}A_i\left[\mu_s\left(1-A_i^2/\alpha_i^2\right)+\eta_i\epsilon\right] - \epsilon\omega_{3\,\mathrm{dB}}\sum_{\substack{j=i-1\\ j\neq i}}^{i+1} A_j\cos(\theta_i-\theta_j+\Phi) \tag{21}$$

$$\frac{\partial\theta_i}{\partial t} = \omega_i + \epsilon\omega_{3\,\mathrm{dB}}\sum_{\substack{j=i-1\\ j\neq i}}^{i+1}\frac{A_j}{A_i}\sin(\theta_i-\theta_j+\Phi), \quad i=1,2,\cdots,N. \tag{22}$$

As in the previous section, for these equations to apply to the end elements in the array, $A_0 = A_{N+1} = 0$ must be defined. This set of equations describes the coupled-oscillator system depicted in Fig. 4.

III. Stable Modes for $\Phi \approx n\pi$

Comparing (14), (15) and (21), (22), one sees that they are virtually identical in form, but differ in the sign of several terms. This small difference can have a profound effect in determining allowed or stable modes of the system.

In previous literature [5], it has been theoretically and experimentally demonstrated that desired phase progressions can be established in nearest-neighbor coupled arrays, using coupling networks like that of Fig. 1(b), by properly detuning the oscillator free-running frequencies prior to synchronization. The coupling phase Φ also plays an important role in determining the stable range of phase shifts and the frequency distribution required for implementation. For example, using (15), it was showed that beam scanning around the broadside direction can be achieved when $\Phi = 0^\circ$ with only detuning of peripheral array elements [6], [7], with the range of stable inter-element phase shifts being $-90^\circ < \Delta\theta < 90^\circ$. Note that the phase dynamics (22) for series-type oscillators with

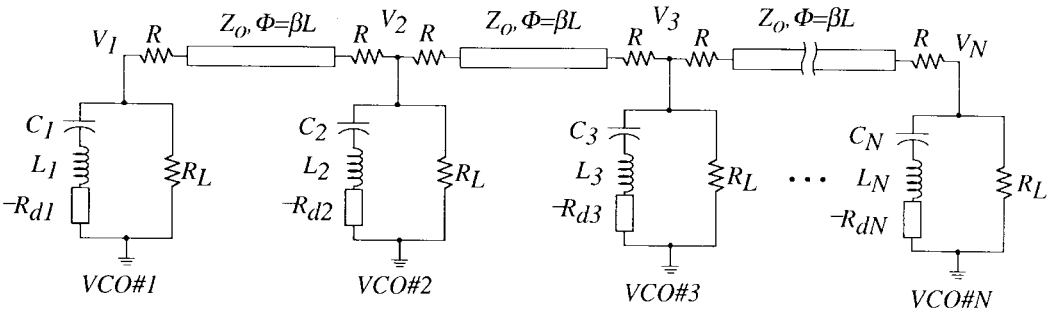

Fig. 4. Schematic diagram of N-parallel-coupled oscillators modeled by series-resonant circuits.

$\Phi = 180°$ would yield exactly the same phase dynamics as the parallel-type (15) with $\Phi = 0°$ (and vice versa). This means that series oscillators require a significantly different coupling circuit than parallel oscillators in order to produce the same phase distributions.

For illustrative purposes, as well as practical merit, the focus, therefore, will be on the case where $\Phi \approx n\pi$—where n is an integer (the following analysis will be accurate for small deviations in coupling phase around the point $\Phi = n\pi$). There will also be interest in the situation involving identical free-running amplitudes and a uniform phase progression, but the analysis will be kept more general when possible.

A. Amplitude Dynamics

Under the conditions $\Phi \approx n\pi$ where n is an integer, the equations governing amplitude dynamics for the two types of oscillators, (14) and (21), can be written in the form

$$\frac{1}{\omega_{3\,\mathrm{dB}}}\frac{\partial A_i}{\partial t} = A_i\mu\left(1 - A_i^2/\alpha_i^2\right) \pm \epsilon\left[\eta_i A_i - \cos\Phi \sum_{\substack{j=i-1 \\ j\neq i}}^{i+1} A_j \cos(\theta_i - \theta_j)\right], \quad i = 1, 2, \cdots, N \tag{23}$$

where the upper sign is for series oscillators and the lower sign is for parallel oscillators.

In general, simultaneous determination of stable steady-state amplitude and phase vectors is difficult. However, in the limit of loose coupling, the amplitude and phase dynamics are essentially decoupled. The steady-state amplitudes can then be determined by a simple Poincaré expansion [9] with respect to the coupling strength ϵ. To first order, this procedure yields

$$A_i \approx \alpha_i \pm \frac{\epsilon\alpha_i}{2\mu}\left[\eta_i - \cos\Phi \sum_{\substack{j=i-1 \\ j\neq i}}^{i+1} \frac{\alpha_j}{\alpha_i}\cos(\theta_i - \theta_j)\right], \quad i = 1, 2, \cdots, N. \tag{24}$$

For the special case of a uniform phase progression and identical free-running amplitudes ($\Delta\phi = \theta_{i+1} - \theta_i$ and $\alpha_i = \alpha$ for all i), the amplitudes are given by

$$A_i \approx \alpha\left\{1 \pm \frac{\epsilon\eta_i}{2\mu}[1 - \cos\Phi\cos\Delta\phi]\right\}, \qquad i = 1, 2, \cdots, N. \tag{25}$$

As long as $\epsilon \ll \mu$, the amplitudes do not significantly deviate from the free-running values. In this case, the stability of the amplitude equations, with respect to small perturbations in either the amplitudes or the phases, will be governed predominantly by the first term in (23), which gives the same constraint as in the free-running case, $\mu > 0$. Therefore, at least in this limit, there is essentially no difference between the series and parallel oscillators as far as the amplitude dynamics are concerned, except for a difference in the sign of the perturbation due to the coupling given by (24). For strong coupling, this argument clearly breaks down, and a more careful consideration of (23) indicates that there is a critical value of coupling for stability, with the series-oscillator arrays becoming unstable at a lower level of coupling strength than the parallel oscillators. However, since these large coupling strengths are accompanied by large amplitude fluctuations and possible multimode phenomena, they are typically avoided in practice. Note also that here, the strength of the coupling is defined relative to the oscillator's amplitude saturation parameter μ. Therefore, it is possible (in principle) to design the oscillators to permit a large coupling strength for enhanced locking bandwidth, but still maintain the condition $\epsilon \ll \mu$ to minimize amplitude fluctuations and maintain stability.

B. Phase Dynamics

Equations (15) and (22) may be cast into a form containing only relative phases by defining

$$\Delta\phi_i \equiv \theta_{i+1} - \theta_i, \quad \Delta\beta_i, \equiv \omega_{i+1} - \omega_i, \qquad i = 1, 2, \cdots, (N-1)$$

which eliminates the problem of having one arbitrary phase and also reduces the order of the system by one. It also eliminates the unknown frequency ω, but after solving for the $\Delta\phi_i$, one can find ω from (15) or (22). Assuming identical free-running amplitudes and $\Phi \approx n\pi$ where n is an integer, the phase equations can be written in matrix form as

$$\frac{d}{dt}\overline{\Delta\phi} = \overline{\Delta\beta} \pm \Delta\omega_m \cos\Phi\, \bar{\bar{A}}\,\bar{s} \tag{26}$$

where $\overline{\Delta\phi}$ and $\overline{\Delta\beta}$ are vectors with elements $\Delta\phi_i$ and $\Delta\beta_i$, $\Delta\omega_m \equiv \epsilon\omega_{3\,\mathrm{dB}}$, and

$$\bar{\bar{A}} = \begin{pmatrix} 2 & -1 & & & 0 \\ -1 & 2 & -1 & & \\ & \ddots & \ddots & \ddots & \\ & & -1 & 2 & -1 \\ 0 & & & -1 & 2 \end{pmatrix}; \quad \bar{s} = \begin{pmatrix} \sin\Delta\phi_1 \\ \sin\Delta\phi_2 \\ \vdots \\ \sin\Delta\phi_{N-1} \end{pmatrix}.$$

The upper sign in (26) is for series oscillators and the lower sign is for parallel oscillators. Setting the time derivative equal to zero gives an algebraic equation for the steady-state phase differences in terms of the oscillator free-running frequencies

$$\bar{s} = \mp\frac{1}{\Delta\omega_m \cos\Phi}\bar{\bar{A}}^{-1}\overline{\Delta\beta} \tag{27}$$

which can be solved by inverting the matrix $\bar{\bar{A}}$ and solving for the phases using the inverse sine function. The upper sign is for series oscillators and the lower sign is for parallel oscillators. Clearly, there are no possible solutions of (27) if any element of the column vector $\bar{\bar{A}}^{-1}\overline{\Delta\beta}$ has a magnitude greater than $\Delta\omega_m|\cos\Phi|$. When there is a valid solution for the sine vector this will correspond to 2^{N-1} different solutions for the phase differences, since the inverse sine function is multivalued. The correct solution is found by stability analysis.

Stability is examined by linearizing (26) around a steady-state solution. Denoting the perturbation to $\overline{\Delta\phi}$ as $\bar{\delta}$ gives

$$\frac{d}{dt}\bar{\delta} = -\bar{\bar{M}}\,\bar{\delta} \tag{28}$$

where the $(N-1)\times(N-1)$ stability matrix $\bar{\bar{M}}$ is

$$\bar{\bar{M}} = \mp\Delta\omega_m \cos\Phi\,\bar{\bar{A}}\,\bar{\bar{C}} \tag{29}$$

and $(N-1)\times(N-1)$ diagonal cosine matrix has been defined as

$$\bar{\bar{C}} = \begin{pmatrix} \cos\Delta\phi_1 & & & 0 \\ & \cos\Delta\phi_2 & & \\ & & \ddots & \\ 0 & & & \cos\Delta\phi_{N-1} \end{pmatrix}.$$

A stable mode requires that all the eigenvalues of $\bar{\bar{M}}$ have positive real parts. This will be true if the matrix is positive definite [10]. The matrix $\bar{\bar{A}}$ is always positive definite, and the matrix $\bar{\bar{C}}$ is also positive definite when each of the phases lies in the range

$$-90^\circ < \Delta\phi_i < 90^\circ, \qquad i = 1, 2, \cdots, (N-1). \tag{30}$$

Since the product of two positive–definite matrices is also positive definite, the eigenvalues of the stability matrix are all real and positive when the phases lie in the above range, as long as $\mp\cos\Phi > 0$. Therefore, (30) represents the stable-phase region for series oscillators when $\Phi = \pi$, and for parallel oscillators when $\Phi = 2\pi$.

Alternatively, the matrix $\bar{\bar{C}}$ is negative definite when each of the phases lies in the range

$$90^\circ < \Delta\phi_i < 270^\circ, \qquad i = 1, 2, \cdots, (N-1) \tag{31}$$

TABLE I
RANGES OF STABLE PHASE SHIFTS FOR DIFFERENT OSCILLATOR MODELS AND COUPLING PHASES CONSIDERED IN THIS PAPER

		Oscillator Model	
		Parallel	Series
Coupling Phase, Φ	$0, 2\pi$	$-90^\circ < \Delta\phi < 90^\circ$	$90^\circ < \Delta\phi < 270^\circ$
	π	$90^\circ < \Delta\phi < 270^\circ$	$-90^\circ < \Delta\phi < 90^\circ$

in which case the eigenvalues of the stability matrix are all real and positive when $\mp\cos\Phi < 0$. Therefore, (31) represents the stable-phase region for series oscillators when $\Phi = 2\pi$, and for parallel oscillators when $\Phi = \pi$.

These results are summarized in Table I. Note that either phase ranges, (30) or (31), are sufficient to cause the vector $\bar{s}$ in (27) to span all of its possible values, which proves that the stability region fills the entire existence region. Furthermore, over this range of phases, the sine functions in $\bar{s}$ are one-to-one. Thus, for each set of tunings within the stability region, there is a unique phase vector which implies that a unique stable synchronized state exists for a given tuning vector $\overline{\Delta\beta}$.

C. Uniform Phase Progression

From (27), one can establish the required conditions for a uniform phase progression $\Delta\phi$ by inserting the $(N-1)$ element sine vector

$$\bar{s} = \sin\Delta\phi(1, 1, \cdots, 1)^T \tag{32}$$

which gives the result

$$\Delta\beta_i = \begin{cases} \Delta\omega_m \sin\Delta\phi, & i = 1 \text{ and } i = N-1 \\ 0, & \text{otherwise.} \end{cases} \tag{33}$$

This implies that a uniform phase shift is induced simply by detuning the end elements of the array (relative to the central elements) by equal amounts, and in opposite directions, with the amount of detuning establishing the amount of the induced phase shift [6], [7]. Inserting the result back into (15) or (22), one finds that the steady-state synchronized frequency is the same as the free-running frequencies of the central elements, independent of the end-element tuning, since the ends are tuned in opposite directions. To summarize, the required frequency distribution is

$$\omega_i = \begin{cases} \omega[1 - \Delta\omega_m \sin\Delta\phi]^{-1}, & \text{if } i = 1 \\ \omega, & \text{if } 1 < i < N \\ \omega[1 + \Delta\omega_m \sin\Delta\phi]^{-1}, & \text{if } i = N. \end{cases} \tag{34}$$

The range of phase shifts which can be synthesized depends on the oscillator model and coupling network as described in Table I. One sees that end-fire or broadside scanning arrays are possible by proper selection of these parameters.

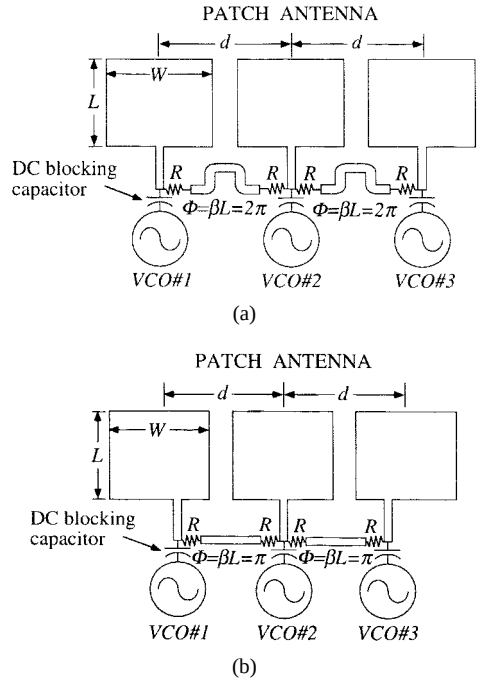

Fig. 5. Diagram illustrating the experimental three-element arrays. (a) Array with one wavelength coupling transmission line ($\Phi = 0, 2\pi$). (b) Array with one-half wavelength coupling transmission line ($\Phi = \pi$). The oscillator in the array can be designed as series-resonant circuit or parallel-resonant circuit.

IV. Experimental Results

The aim of this paper's experiments was to verify the derived coupling stability results summarized in Table I. Four three-element linear-coupled-oscillator arrays were built: two arrays were constructed with a coupling phase of $\Phi = \beta L = 2\pi$ [Fig. 5(a)] and two with $\Phi = \beta L = \pi$ [Fig. 5(b)]. In each of the two cases, series- or parallel-resonator oscillators were used. The circuits were fabricated on 0.787-mm-thick Rogers Duroid board 5880 ($\epsilon_r = 2.2$). The voltage-controlled oscillators (VCO's) in the arrays were coupled together by 75-Ω microstrip transmission lines, resistively loaded with two 120-Ω chip resistors, as shown in Fig. 5. The coupling phase was manipulated by varying the length of the line. The series-resonator oscillators were designed to operate at a common frequency of 10.7 GHz, while the parallel-resonator oscillators operated at 10.5 GHz. The VCO's used NE32184A packaged MESFET's as the active device and MA-COM 46 580 varactor diodes for tuning. A series model was obtained by terminating the source and gate terminals and feeding a load from the drain terminal; a simulation of the small-signal equivalent circuit looking into the drain terminal for this circuit is shown in Fig. 6, clearly indicating a series resonance. Alternatively, a parallel model was obtained by terminating the drain and gate and feeding a load from the source terminal; the small-signal simulation for this circuit is shown in Fig. 7, indicating a parallel equivalent. In each case, over 1-GHz tuning range was obtained around the center frequencies.

Each VCO delivered power to a patch antenna, 11.8-mm wide and 9.3-mm long, which employed a quarter-wave matching network to present a 20-Ω resonant load to the oscillator circuit. The antenna spacing d was 14 mm, which is about

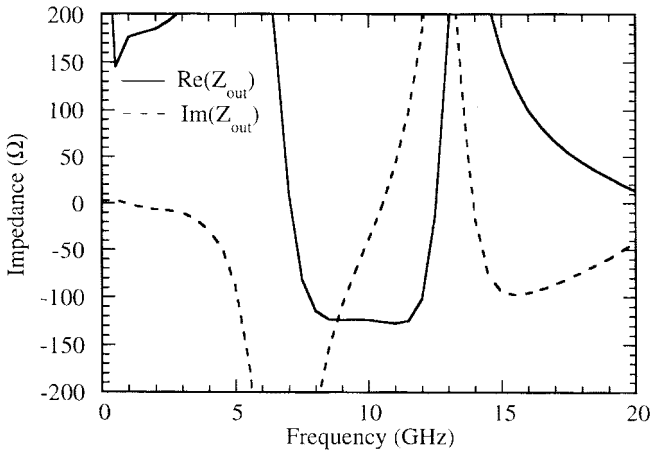

Fig. 6. Simulation result of the output impedance of the oscillator with series-resonant circuit near the oscillating frequency. The result is generated by EEsof LIBRA program.

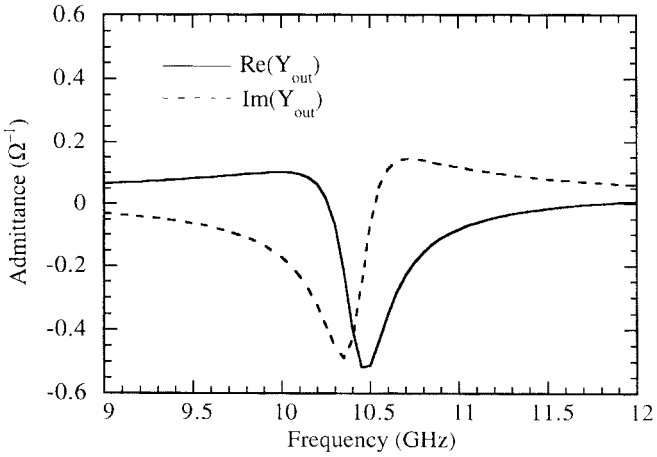

Fig. 7. Simulation result of the output admittance of the oscillator with parallel-resonant circuit near the oscillating frequency. The result is generated by EEsof LIBRA program.

half the free-space wavelength at the oscillation frequency. The locking ranges for the series-resonator and parallel-resonator networks were 110 and 40 MHz, respectively. In the arrays with $\Phi = 180°$, the feedpoints of the patch antenna are offset from the center positions due to the limits imposed by the patch-antenna sizes and spacing. However, measurements of the input impedance of the patch antennas with offset feed positions indicated that the input impedance was relatively unchanged within the desired oscillation frequency ranges. The Q-factors of the oscillators was much larger than that of the patch antenna within the tuning range of the VCO, which is a necessary condition for validity of the theory.

The measured (H-plane) radiation patterns for the four three-element arrays are shown in Figs. 8–11. As described in Section III-C, the phase progression in the array can be changed by detuning the free-running frequencies of both end elements in opposite directions. It can be seen that the elements of series-resonator model with $\Phi = \pi$ (Fig. 8) and those of parallel resonators with $\Phi = 2\pi$ (Fig. 9) both resulted in scanning around the broadside position, consistent with the range of allowed phase shifts in Table I for this case. In

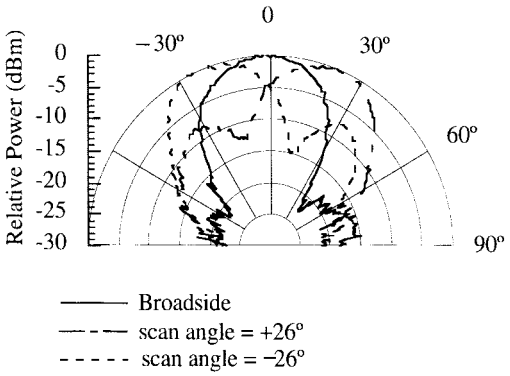

Fig. 8. Measured radiation pattern of three-element coupled oscillators designed as series-resonant circuits with $\Phi = \pi$. The array is locked to the common frequency 10.7 GHz. The result shows broadside patterns and maximally scanned patterns at $\pm 26^\circ$, which are close to the theory values $\pm 30^\circ$ based on the phase in Table I for this case.

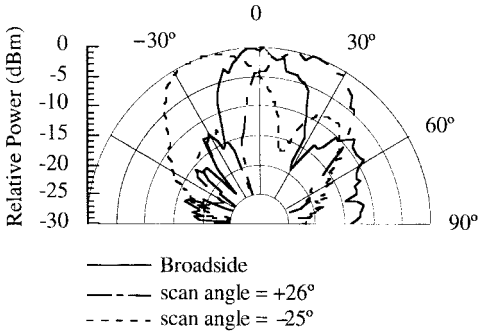

Fig. 9. Measured radiation pattern of three-element coupled oscillators designed as parallel-resonant circuits with $\Phi = 0, 2\pi$. The array is locked to the common frequency 10.5 GHz. The result shows broadside patterns and maximally scanned patterns at $+26^\circ$ and -25°, which are close to the theory values $\pm 30^\circ$ based on the phase in Table I for this case.

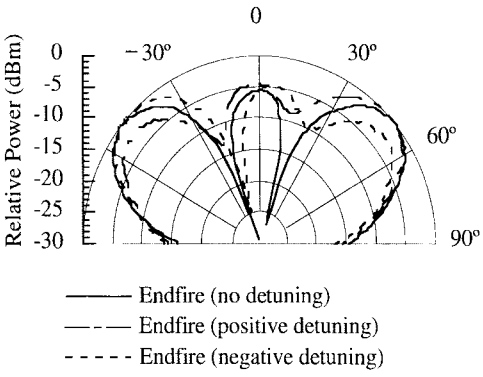

Fig. 10. Measured radiation pattern of three-element coupled oscillators designed as series-resonant circuits with $\Phi = 0, 2\pi$. The array is locked to the common frequency 10.7 GHz. The result shows patterns with and without detuning, which are consistent with the theoretical allowed phases in Table I.

Figs. 8 and 9, the measured radiation patterns for maximum detuning are close to the theoretical value of $\pm 30^\circ$ [4]–[7]. The remaining arrays (Figs. 10 and 11) resulted in patterns consistent with end-fire phasing, as expected from Table I. (Naturally, the shape of the single-patch H-plane pattern does not allow for true end-fire patterns.) These results, therefore, verify that it is both the resonator model and coupling phase which determines the stable range of achievable phase shifts.

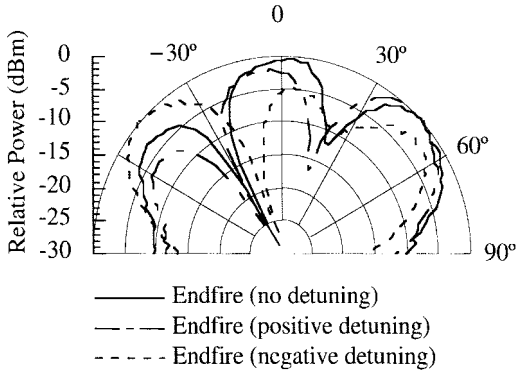

Fig. 11. Measured radiation pattern of three-element coupled oscillators designed as parallel-resonant circuits with $\Phi = \pi$. The array is locked to the common frequency 10.5 GHz. The result shows patterns with and without detuning, which are consistent with the theoretical allowed phases in Table I.

V. Conclusion

In this paper, the dependence of the dynamics of parallel-coupled oscillators on the equivalent circuit of the oscillator, and the coupling phase between the elements have been examined. The oscillator can be modeled using either a series- or parallel-resonator circuit. Significant differences are found in the dynamics for a given coupling scheme, leading to different stable-phase distributions for each case. The analysis specifically focuses on a simple nearest-neighbor coupling topology used in previous analytical and experimental literature [5]. The theory is verified using four separate three-element MESFET oscillator arrays at X-band, which represent the four permutations of either series or parallel equivalents and two different coupling configurations.

Acknowledgment

The authors wish to acknowledge NEC and the California Eastern Laboratories for donating the MESFET devices, and Rogers Corp. for donating the Duroid substrates used in this paper.

References

[1] K. D. Stephan, "Inter-injection-locked oscillators for power combining and phased arrays," *IEEE Trans. Microwave Theory Tech.*, vol. MTT-34, pp. 1017–1025, Oct. 1986.

[2] K. D. Stephan and W. A. Morgan, "Analysis of inter-injection-locked oscillators for integrated phased arrays," *IEEE Trans. Antennas Propagat.*, vol. AP-35, pp. 771–781, July 1987.

[3] J. Lin, S. T. Chew, and T. Itoh, "A unilateral injection-locking type active phased array for beam scanning," in *IEEE MTT-S Int. Microwave Symp. Dig.*, San Diego, CA, June 1994, pp. 1231–1234.

[4] R. A. York, "Nonlinear analysis of phase relationships in quasi-optical oscillator arrays," *IEEE Trans. Microwave Theory Tech.*, vol. 41, pp. 1799–1809, Oct. 1993.

[5] R. A. York, P. Liao, and J. J. Lynch, "Oscillator array dynamics with broadband N-port coupling networks," *IEEE Trans. Microwave Theory Tech.*, vol. 42, pp. 2040–2045, Nov. 1994.

[6] P. Liao and R. A. York, "A new phase-shifterless beam-scanning technique using arrays of coupled oscillators," *IEEE Trans. Microwave Theory Tech.*, vol. 41, pp. 1810–1815, Oct. 1993.

[7] P. Liao and R. A. York, "A six-element scanning oscillator array," *IEEE Microwave Guided Wave Lett.*, vol. 4, pp. 20–22, Jan. 1994.

[8] J. J. Lynch, "Analysis and design of systems of coupled microwave oscillators," Ph.D. dissertation, Dept. Elect. Eng., Univ. California at Santa Barbara, Jan. 1996.

[9] F. Verhulst, *Nonlinear Differential Equations and Dynamical Systems*. Berlin, Germany: Springer, 1990.

[10] C. R. Wylie and L. C. Barrett, *Advanced Engineering Mathematics*, 5th ed. New York: McGraw Hill, 1982.

Heng-Chia Chang received the B.S. degree in electrical engineering from National Taiwan University, Taipei, Taiwan, R.O.C., in 1990, and M.S. degree in electrical and computer engineering from the University of California at Santa Barbara (UCSB), in 1994, where he is currently working toward the Ph.D. degree.

From 1990 to 1992, he served in the Taiwan Air Force as a Technical Officer, where he received maintenance training for various wireless communication systems, such as the GCA radar system, digital fiber-optical communication system, telephones, and digital PABX system. His current research interests include noise analysis, nonlinear-microwave-circuit design, coupled-oscillator theory, nonlinear optics, and statistical optics.

Eric S. Shapiro (S'95–M'96) received the B.S. degree (hon) in electrical engineering from the University of California (UCSB) at Santa Barbara, in 1996. He joined the Wave Electronics Group at UCSB, in 1996, and is working toward his M.S. thesis in microwave power combining.

His current research interests include power combining techniques and RF and microwave communication circuits and subsystems.

Mr. Shapiro is a member of Eta Kappa Nu and Tau Beta Pi, and was a recipient of an Andersen Consulting Outstanding Junior Award for Scholarship, Leadership, and Fellowship.

Robert A. York (S'85–M'89) received the B.S. degree in electrical engineering from the University of New Hampshire, Durham, in 1987, and the M.S. and Ph.D. degrees in electrical engineering from Cornell University, Ithaca, NY, in 1989 and 1991, respectively.

He is currently an Associate Professor of electrical and computer engineering at the University of California at Santa Barbara (UCSB). His group at UCSB is currently involved with the design and fabrication of microwave and millimeter-wave circuits, microwave photonics, high-power microwave and millimeter-wave modules using spatial combining and wide-bandgap semiconductor devices, and time-domain modeling of antennas, power-combining arrays, and other electromagnetic or electronic structures.

Dr. York received the Army Research Office Young Investigator Award in 1993, and the Office of Naval Research Young Investigator award in 1996.